Supplemental information

The Spontaneous Cascade Optimization Strategy of the Double Enrichment Improves Anion-Derived Solid Electrolyte Interphases to Enable Stable Lithium-Metal Batteries

Fengxu Zhen[1+], Hong Liu[1+], Yingbin Wu[1+], Xinjia Zhou[1], Weiping Li[1], Yuzhi Chen[1], Yuke Zhou[1], Haoyang Wang[1], Xiangkai Yin[1], Shujiang Ding[1,*], Xiaodong Chen[2,*], Wei Yu[1,*]

[1]School of Chemistry, Engineering Research Center of Energy Storage Materials and Devices, Ministry of Education, Xi'an Jiaotong University, Xi'an, 710049, P. R. China.

[2]Xi'an Institute of Optical Precision Machinery, Chinese Academy of Sciences, Xi'an Shanxi 710000 (P. R. China)

*Corresponding author. E-mail: dingsj@mail.xjtu.edu.cn, yuwei2019@mail.xjtu.edu.cn, cxd_1979@163.com

Table of Contents

Supplementary Figures

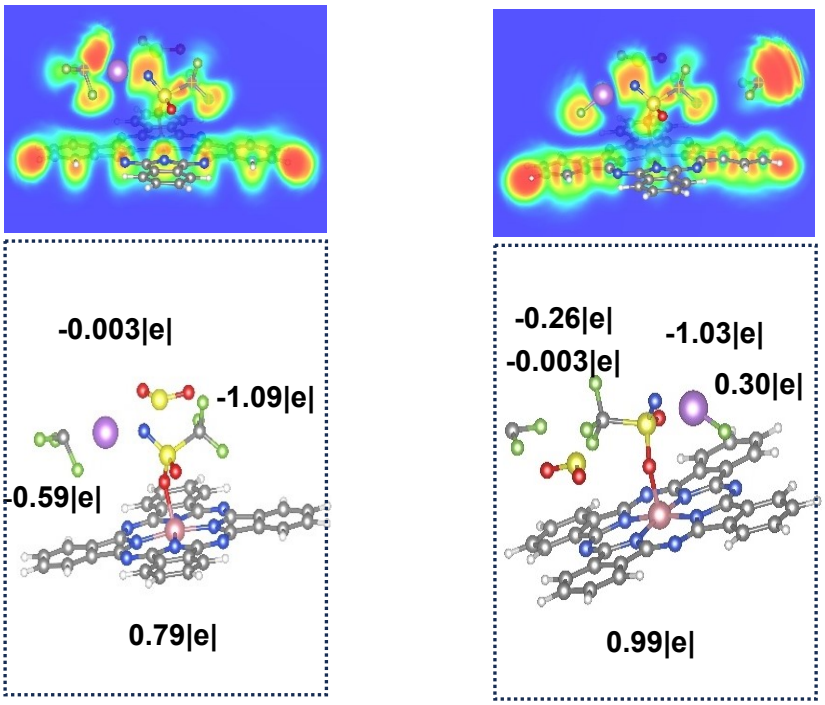

Fig. S1 DFT simulations with Bader charge (measured in units of |e|) illustrate the degradation dynamics of $TFSI^-$, along with the corresponding ELF of $TFSI^-$ at various steady states (final two steps).

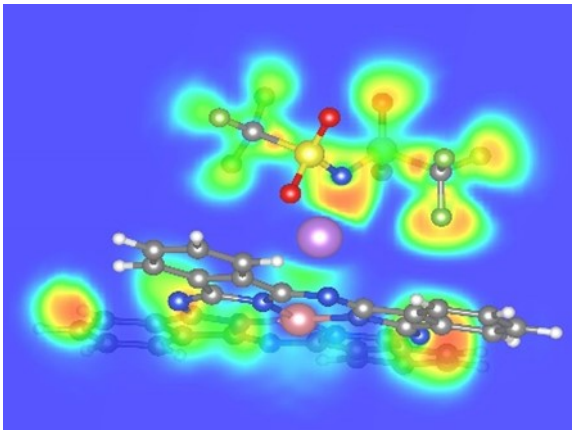

Fig. S2 DFT calculations to analyze the effect of cobalt phthalocyanine on C-F chemical bonding in LiTFSI.

(a)

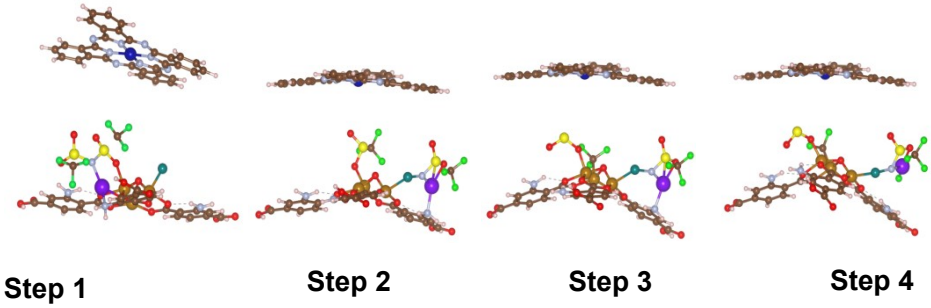

(b)

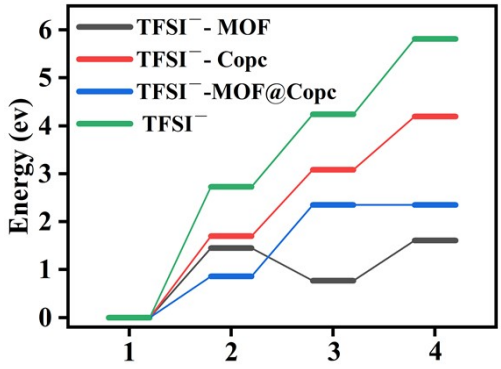

Figure S3. (a,b) DFT calculations to analyze the magnitude of energy barriers for the four-step reaction of cobalt phthalocyanine, NH_2-MIL-101(Fe), and composites to LiTFSI.

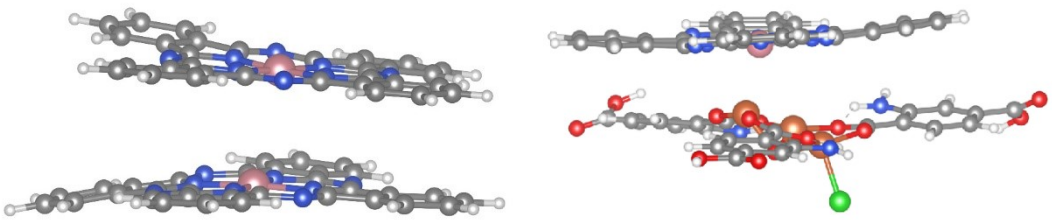

E_{ads} (Copc- Copc) =-0.11 eV **E_{ads} (MOF-Copc) =-0.63 eV**

Figure S4. (a) The binding energy of MOF and Copc. (b) Binding energy within two Copc molecules.

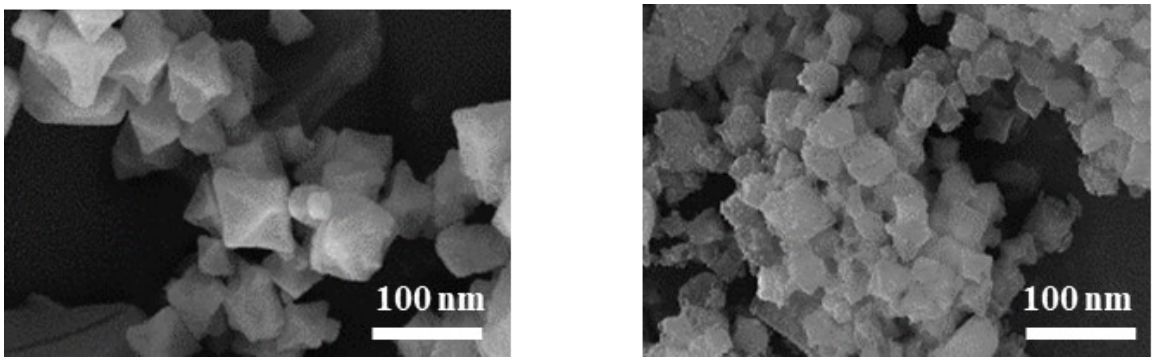

Figure S5. SEM images of MOF and MOF@Copc.

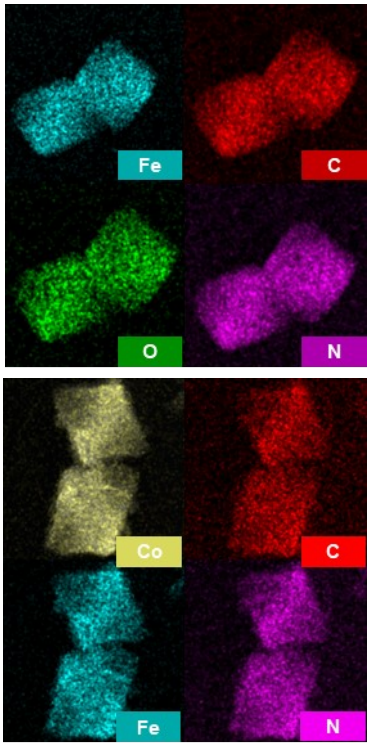

Figure S6. TEM elemental mapping of NH_2-MIL-101(Fe) and NH_2-MIL-101(Fe)@CoPc.

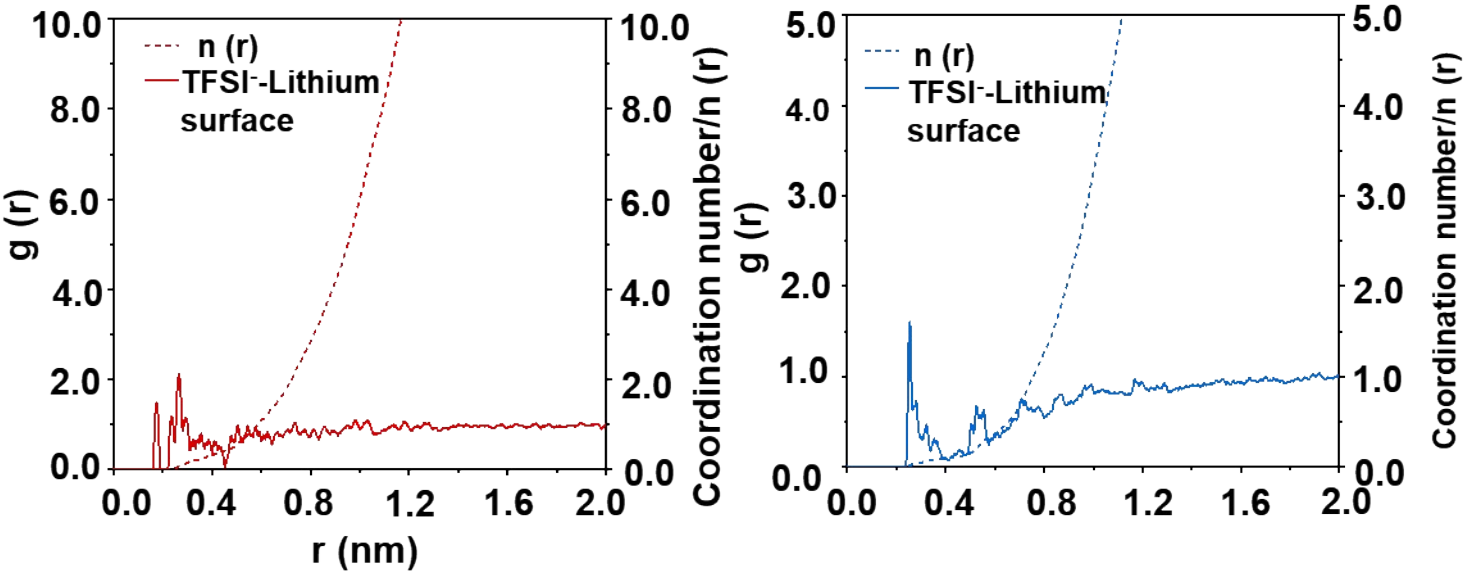

Figure S7. Radial distribution function diagram of Li modified by MOF and bare Li.

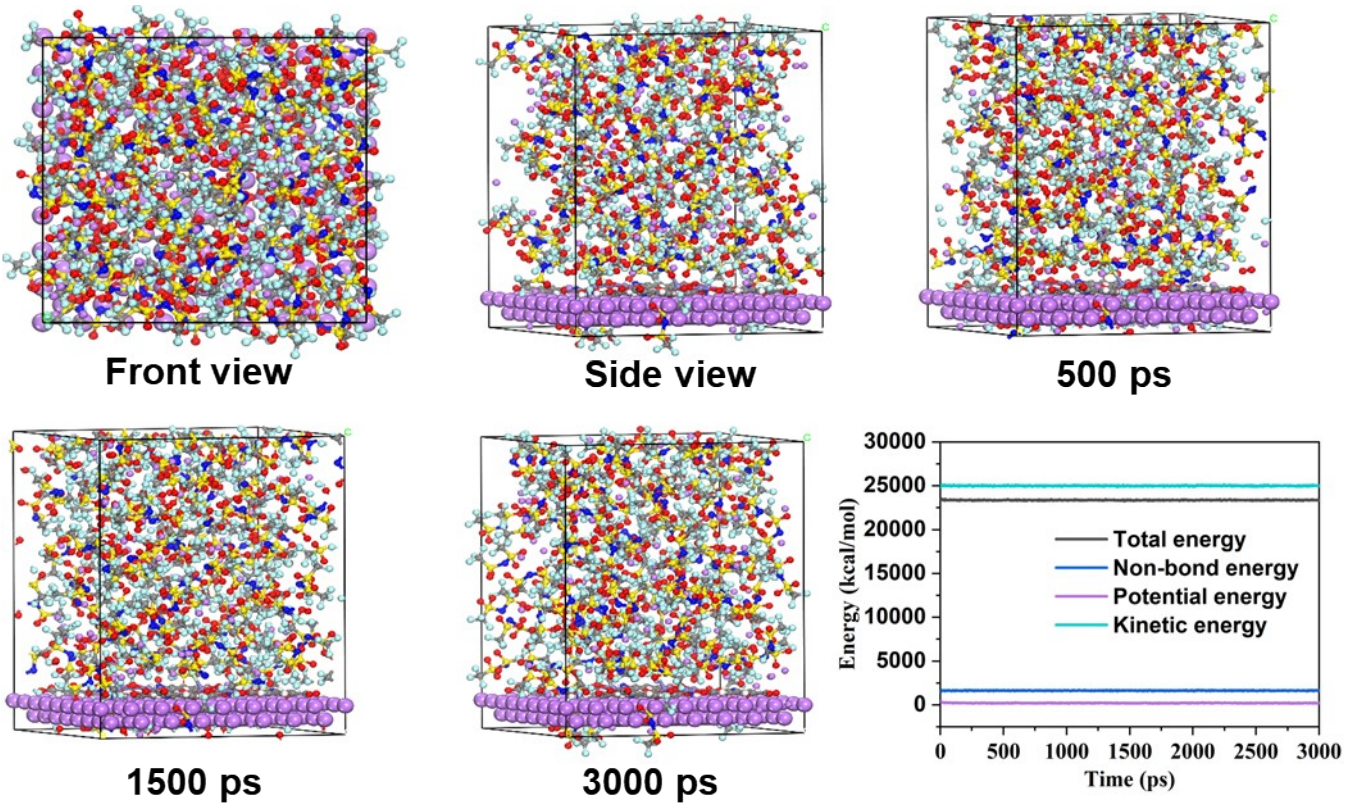

Figure S8. The snapshots of molecular dynamics of Bare Li and energies of molecular dynamics simulations.

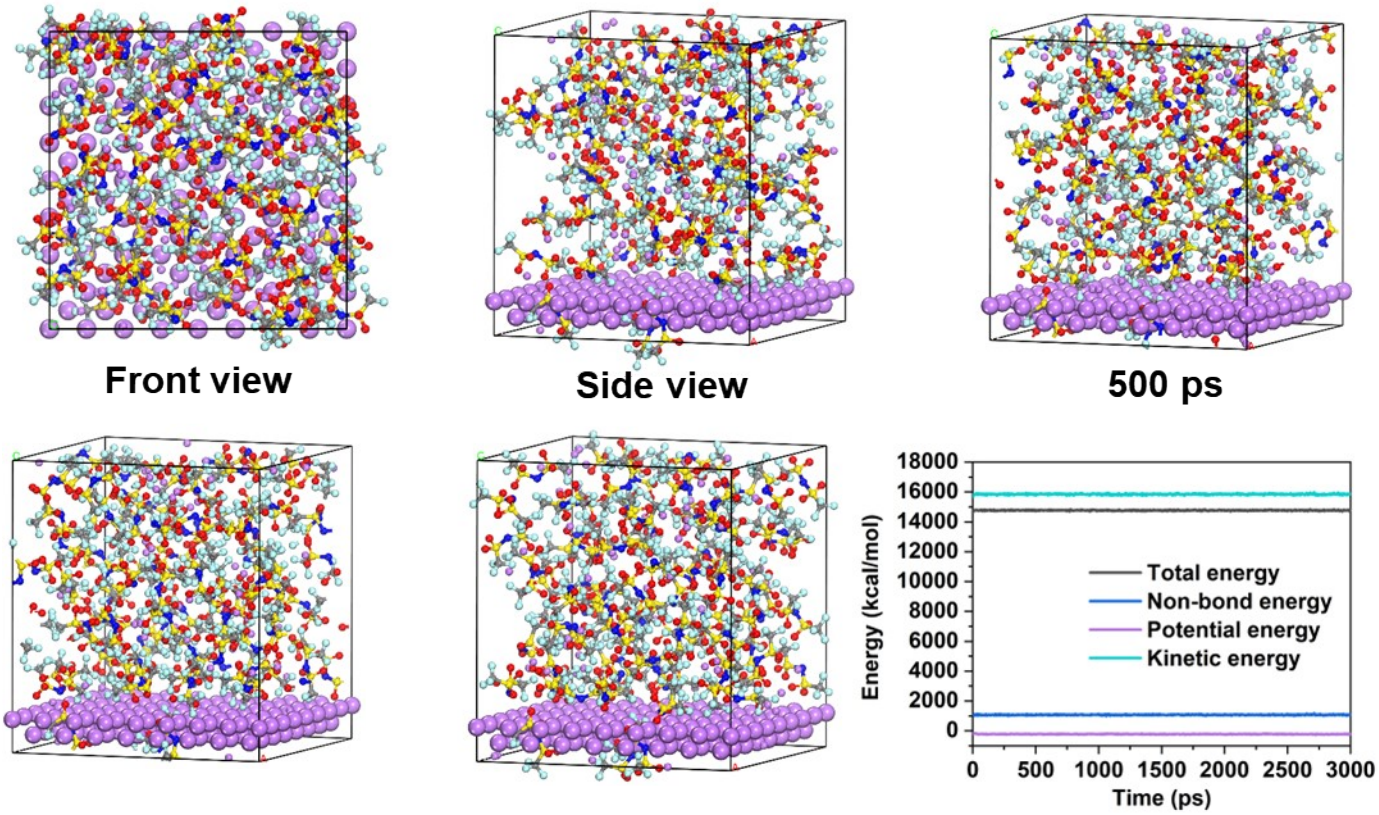

Figure S9. The snapshots of molecular dynamics of MOF/Li and energies of molecular dynamics simulations

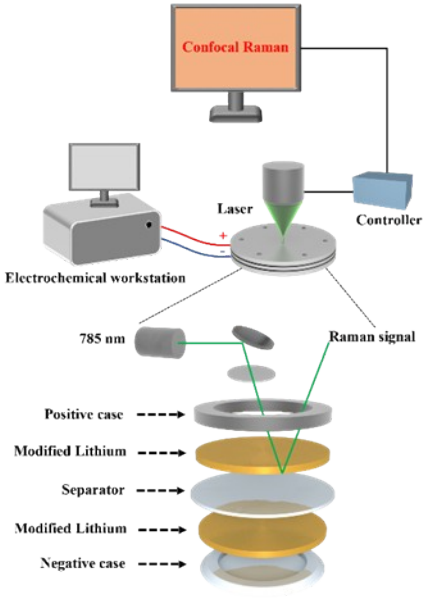

Figure S10. Schematic diagram of the in-situ Raman device.

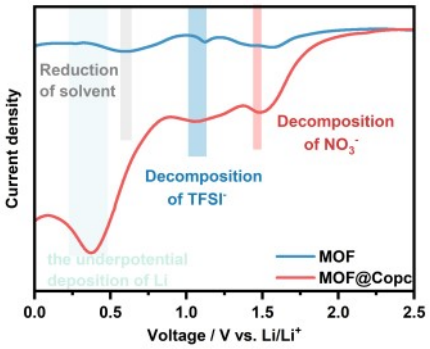

Figure S11. The CV curves of lithium metal cells were modified with MOF and MOF@Copc at a certain scan rate.

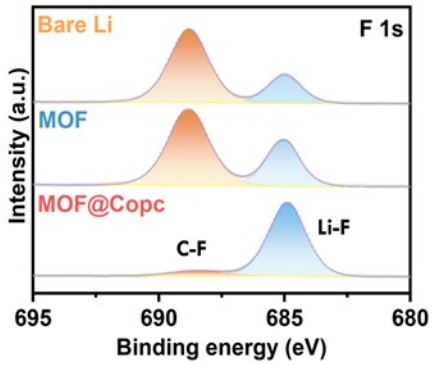

Figure S12.XPS spectra of F 1s for bare Li, MOF/Li, and MOF@Copc/Li electrodes.

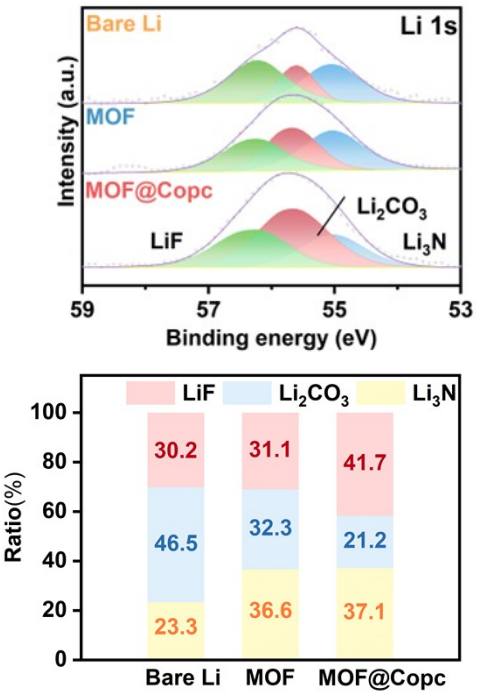

Figure S13. XPS spectra of Li 1s for bare Li, MOF/Li, and MOF@Copc/Li electrodes- relative contents of LiF, Li_3N, and $LiCO_3$.

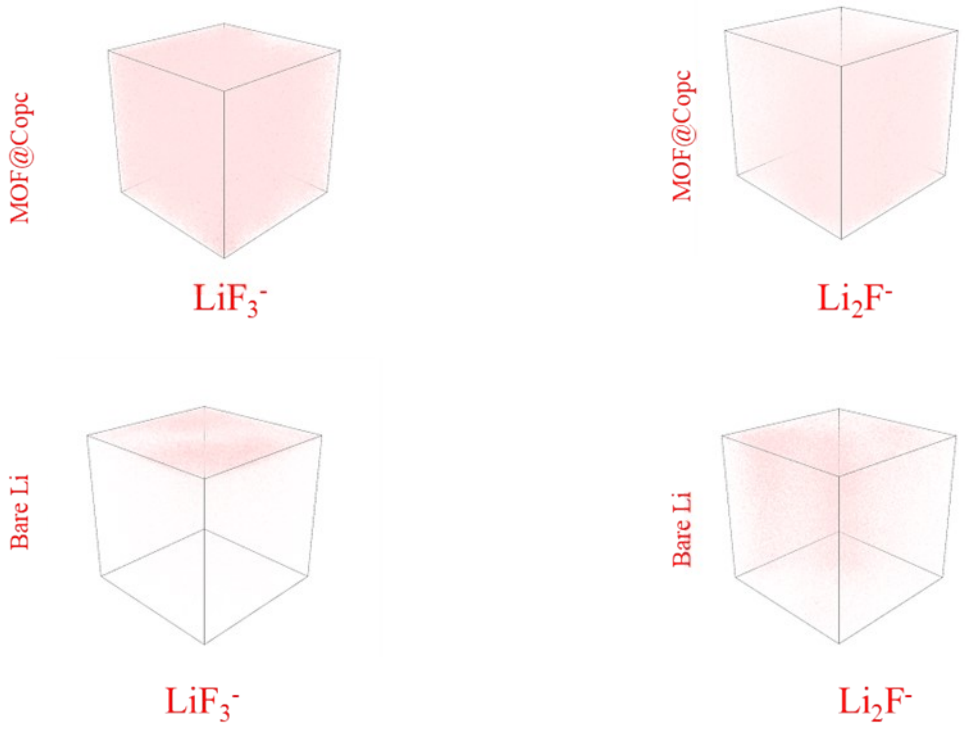

Figure S14. Structures of Bare Li and MOF@Copc-modified lithium battery-derived SEIs studied by TOF-SIMS.

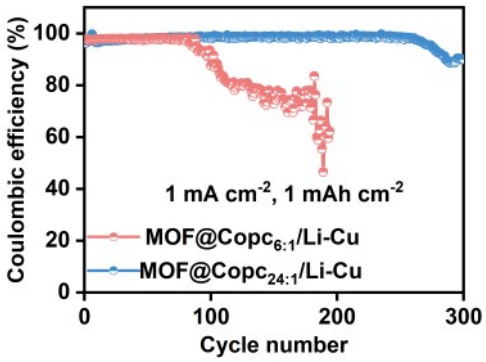

Figure S15. Battery cycling performance of asymmetric Li-Cu half-cells modified with mass ratios MOF: Copc = 6:1 and 24:1.

We found that excessive Copc results in significant aggregation, which prevents the formation of a uniform coating; conversely, insufficient Copc fails to form a better SEI. Comparative tests

demonstrated that the MOF@Copc composite material achieves optimal performance at a mass ratio of 12:1.

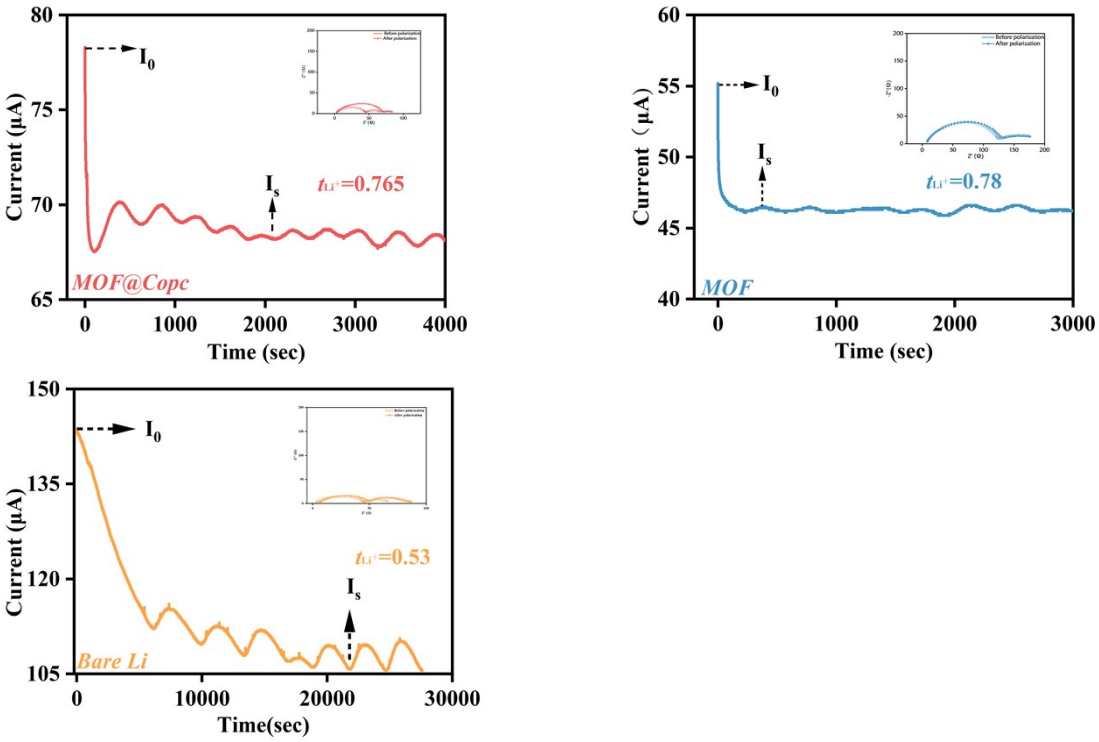

Figure S16. Lithium-ion mobility of Bare Li, MOF/Li, and MOF@Copc.

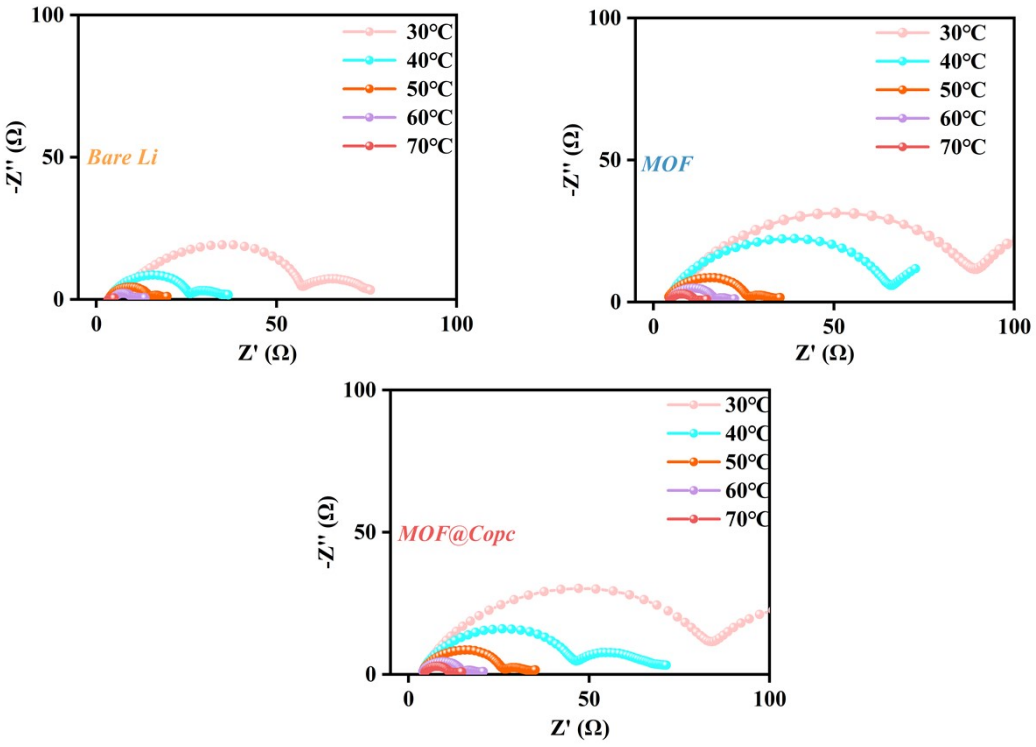

Figure S17. Impedance magnitude of Li||Li symmetric cells at different temperatures.

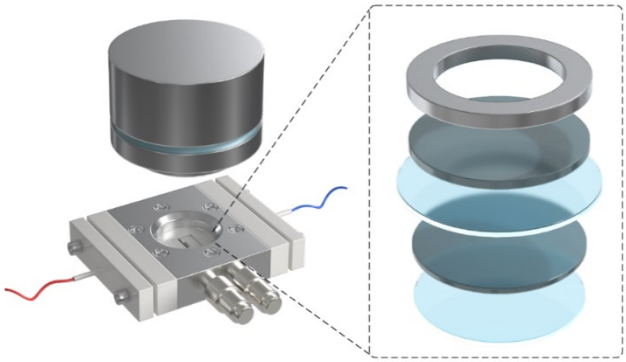

Figure S18. Schematic diagram of the in-situ optical microscope.

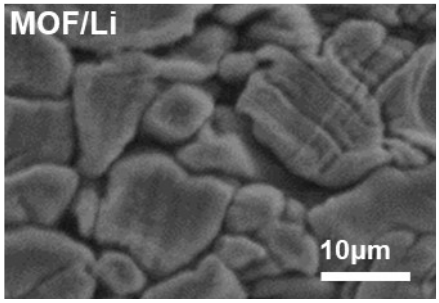

Figure S19. Corresponding SEM images after plating for MOF/Li.

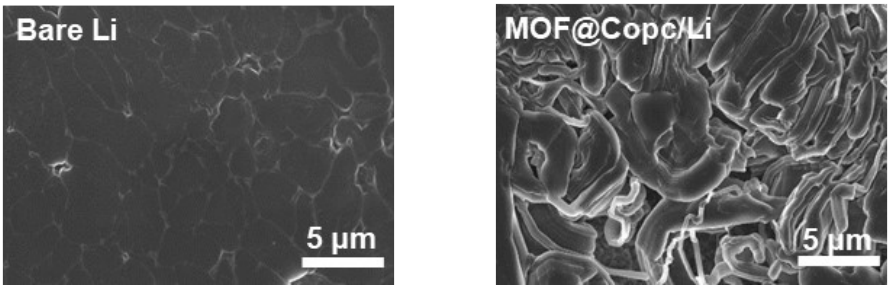

Figure S20. The fiftieth circle deposition SEM images of MOF@Copc/Li and Bare Li at a current

density of 3 mA cm^{-2} and a capacity of 3 mAh cm^{-2}.

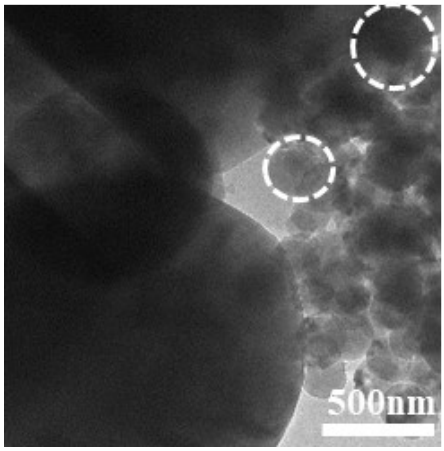

Figure S21. Lithium deposition morphology under cryo-electron microscopy.

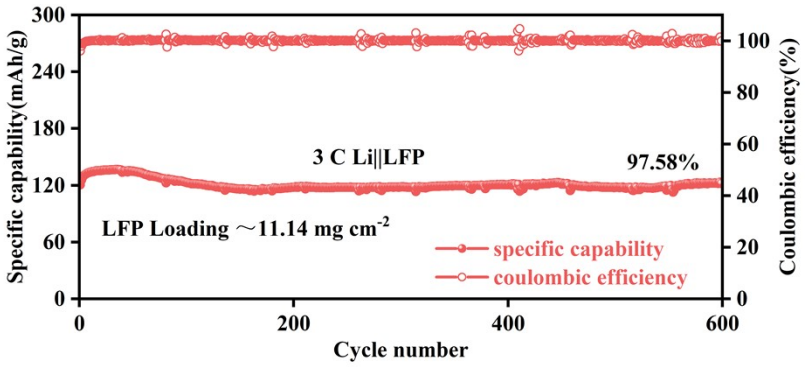

Figure S22. Full-cell cycling performance of MOF@Copc/Li||LFP (high loading) at 3C conditions.

(a)

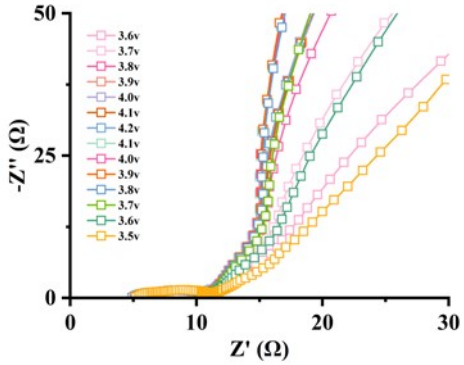

(b)

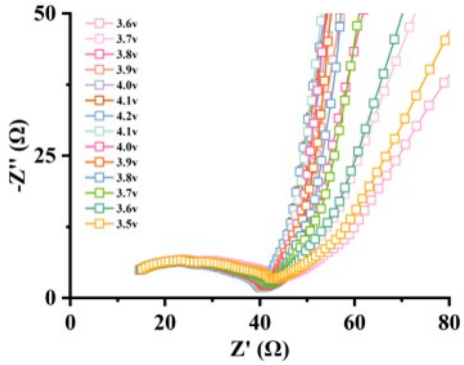

Figure S23. Impedance values at different voltages (a)MOF@Copc(b) bare Li

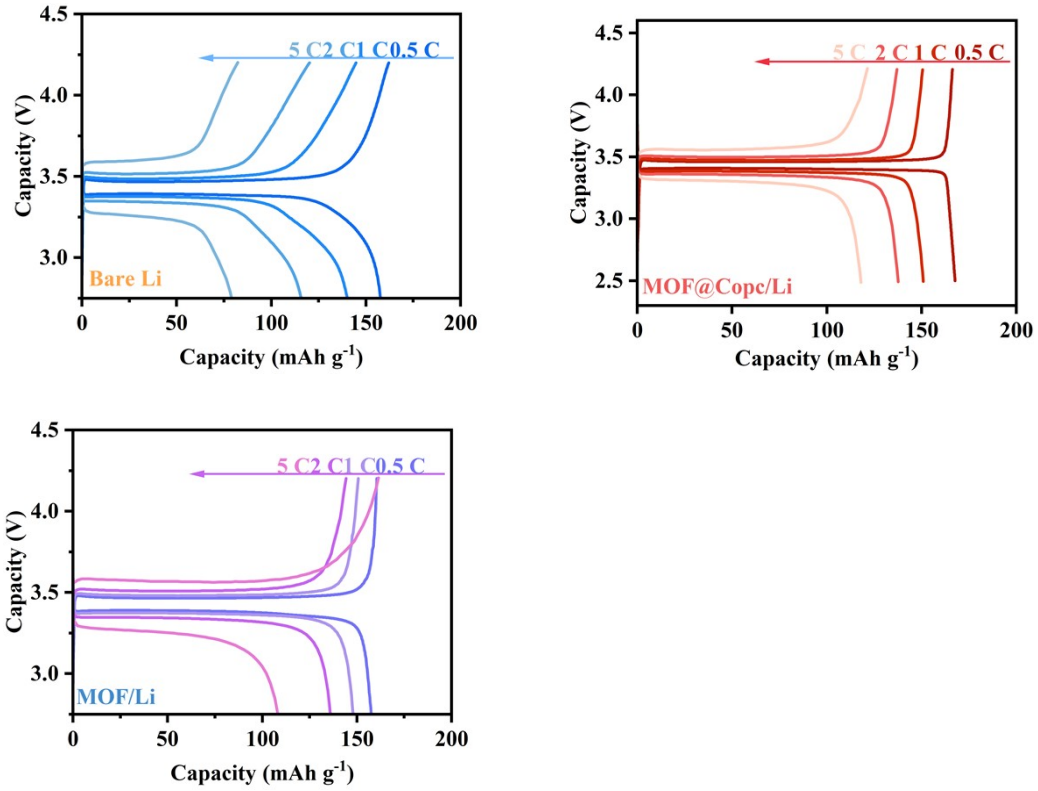

Figure S24. Corresponding galvanostatic charge-discharge curves of LFP-MOF@Copc/Li, LFP-MOF/Li, and LFP-bare Li cells at increasing rates from 0.5 to 5 C.

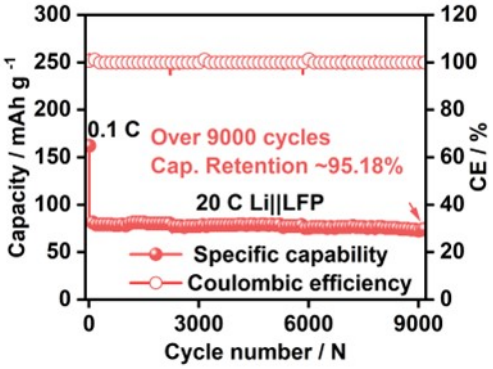

Figure S25. Cycling performances of LFP-MOF@Copc/Li cells at 20 C high rate.

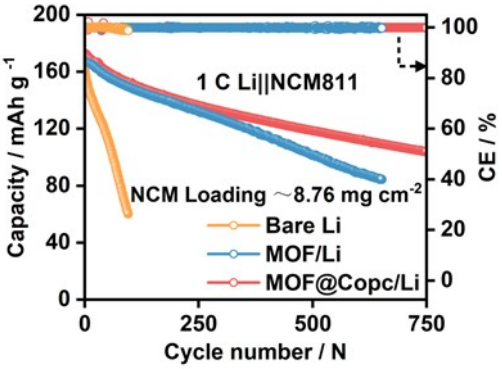

Figure S26. Cycling performances of NCM811-MOF@Copc/Li, NCM811-MOF/Li, and NCM811-bare Li cells at 1 C rate.

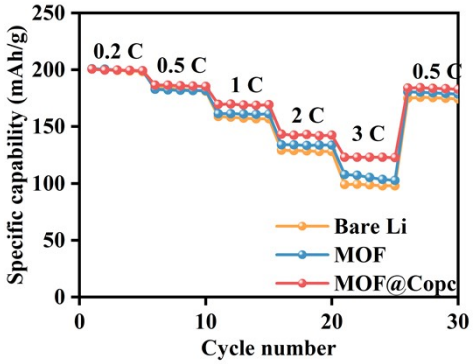

Figure S27. Corresponding galvanostatic charge-discharge curves of NCM811-MOF@Copc/Li, NCM811-MOF/Li, and NCM811-bare Li cells at increasing rates from 0.2 to 3 C (High loading 8.76 mg cm^{-2}).

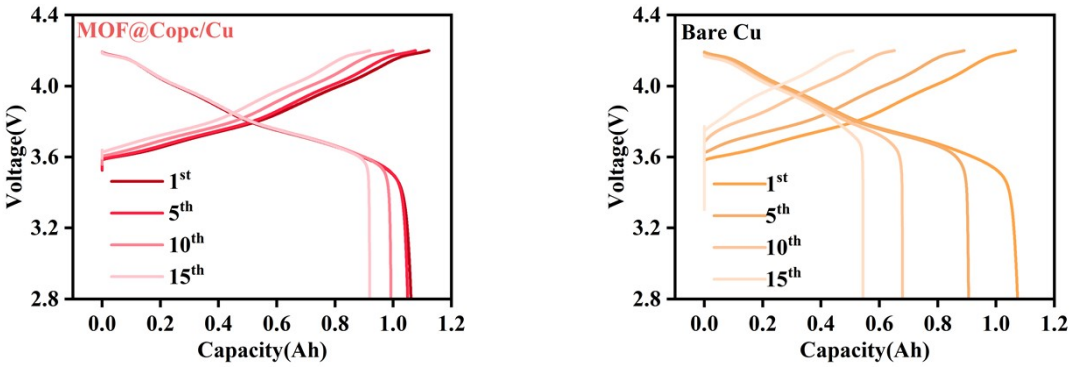

Figure S28. The capacity-voltage curve of MOF@Copc/Cu|| NCM811 and Cu|| NCM811 pouch battery.

Table S1. Size of the bond length of the C-F bond chemical bond

Chemical formula		C-F bond lengths (Å)	
C-F species	F1-C bond	F2-C bond	F3-C bond
$TFSI^-$	1.343	1.344	1.346
Final state	1.363	1.351	1.350

Condition	Energy Barrier (eV)
Free $TFSI^-$	**2.72**
CoPc on free $TFSI^-$	**1.69**
MOF-Fixed $TFSI^-$	**1.45**
Copc on MOF-Fixed $TFSI^-$	**1.21**

Table S2. The magnitude of the energy barrier (eV).